Neuroradiology Case of the Day

Charles F. Lanzieri[1], Barbara A. Bangert, Robert W. Tarr, Rakesh S. Shah, Jonathan S. Lewin, Robert C. Gilkeson

Case 1

A 14-year-old girl with partial complex seizures.

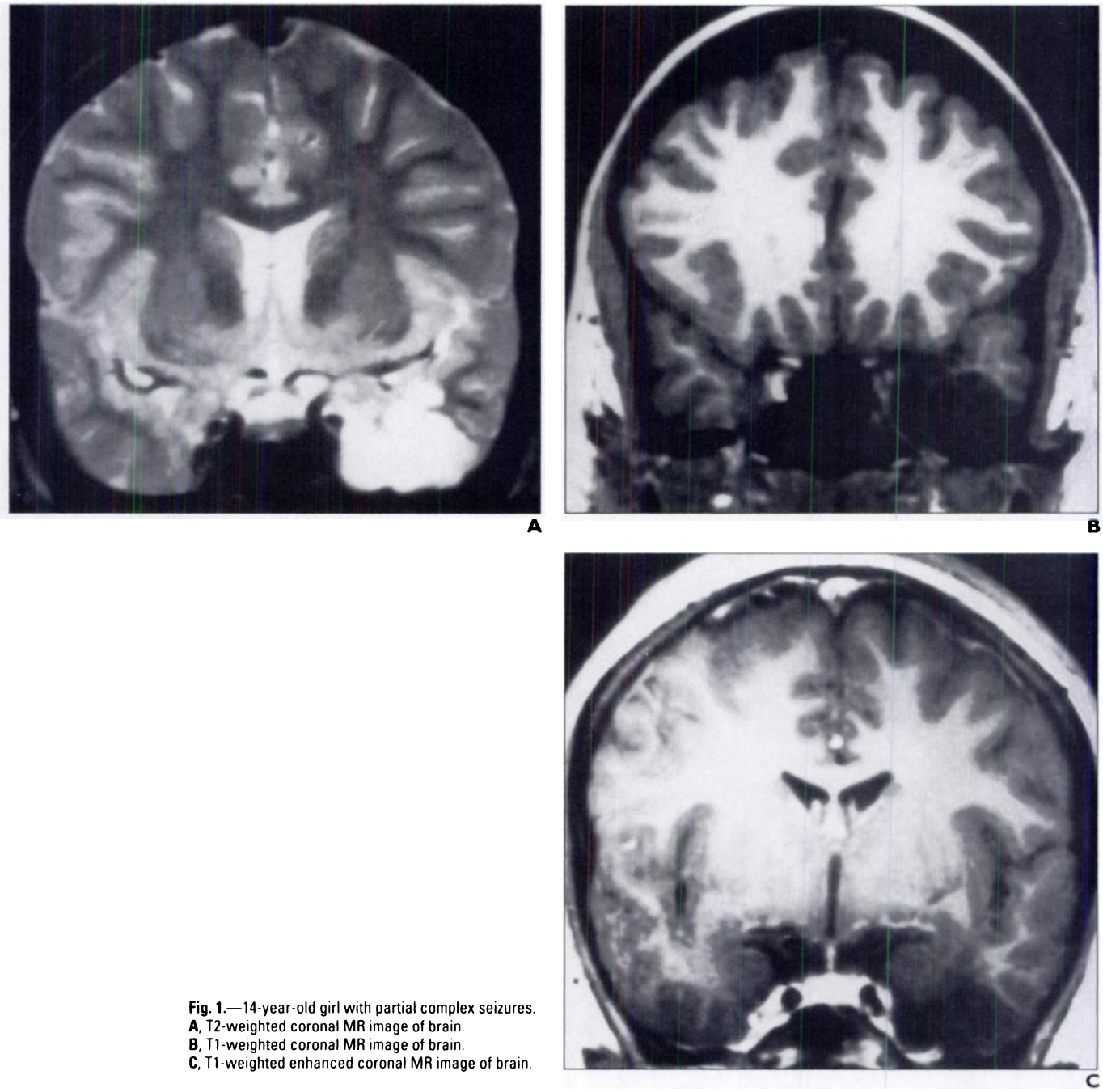

Fig. 1.—14-year-old girl with partial complex seizures.
A, T2-weighted coronal MR image of brain.
B, T1-weighted coronal MR image of brain.
C, T1-weighted enhanced coronal MR image of brain.

[1]All authors: Department of Radiology, University Hospitals of Cleveland, 11100 Euclid Ave., Cleveland, OH 44106. Address correspondence to C. F. Lanzieri.

AJR 1997;169:293–302 0361–803X/97/1691–293 © American Roentgen Ray Society

Case 2

A 20-year-old man with a 3-week course of progressive headache, visual loss, and 30-lb (14-kg) weight loss. During that time, he also developed migratory numbness of the right side of his body and weakness of the right upper and lower extremities.

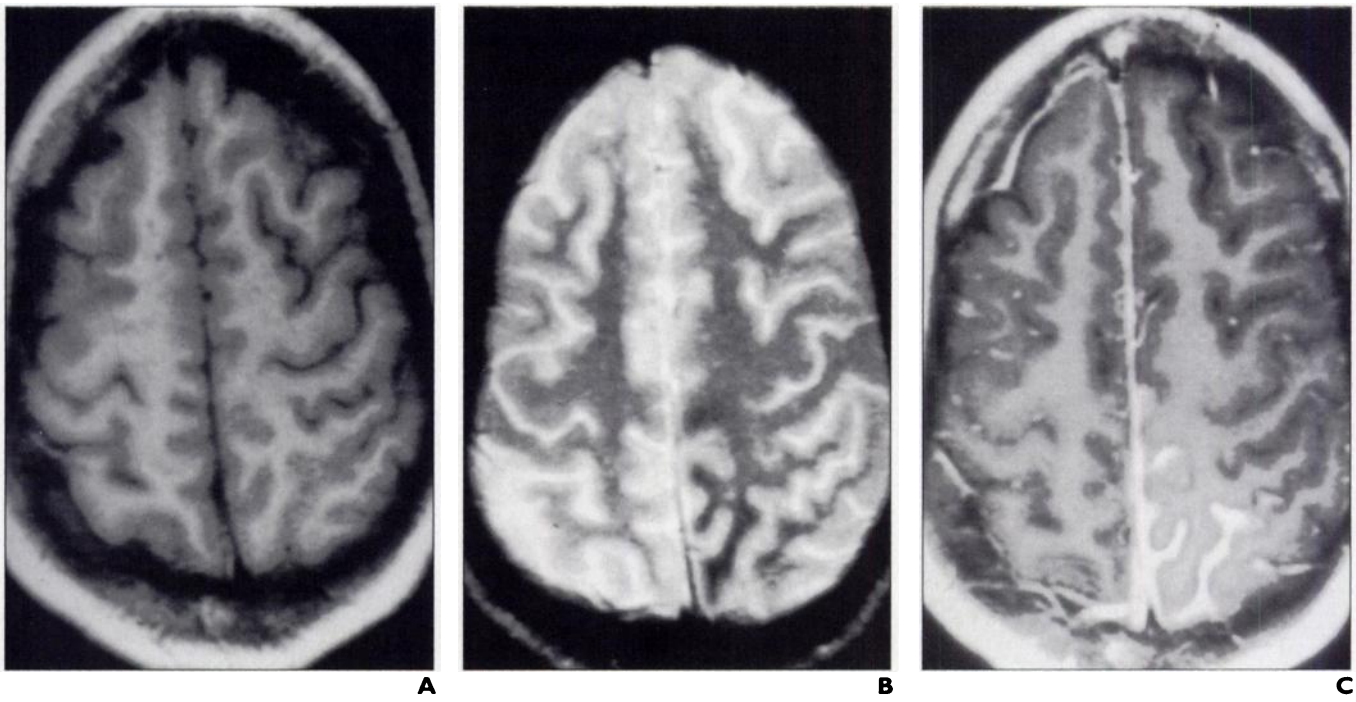

Fig. 2.—20-year-old man with 3-week course of progressive headache, visual loss, and 30-lb (14-kg) weight loss.
A, T1-weighted axial MR image of brain.
B, T2-weighted axial MR image of brain.
C, Contrast-enhanced axial T1-weighted MR image of brain.

Case 3

A 29-year-old HIV-positive man with headache.

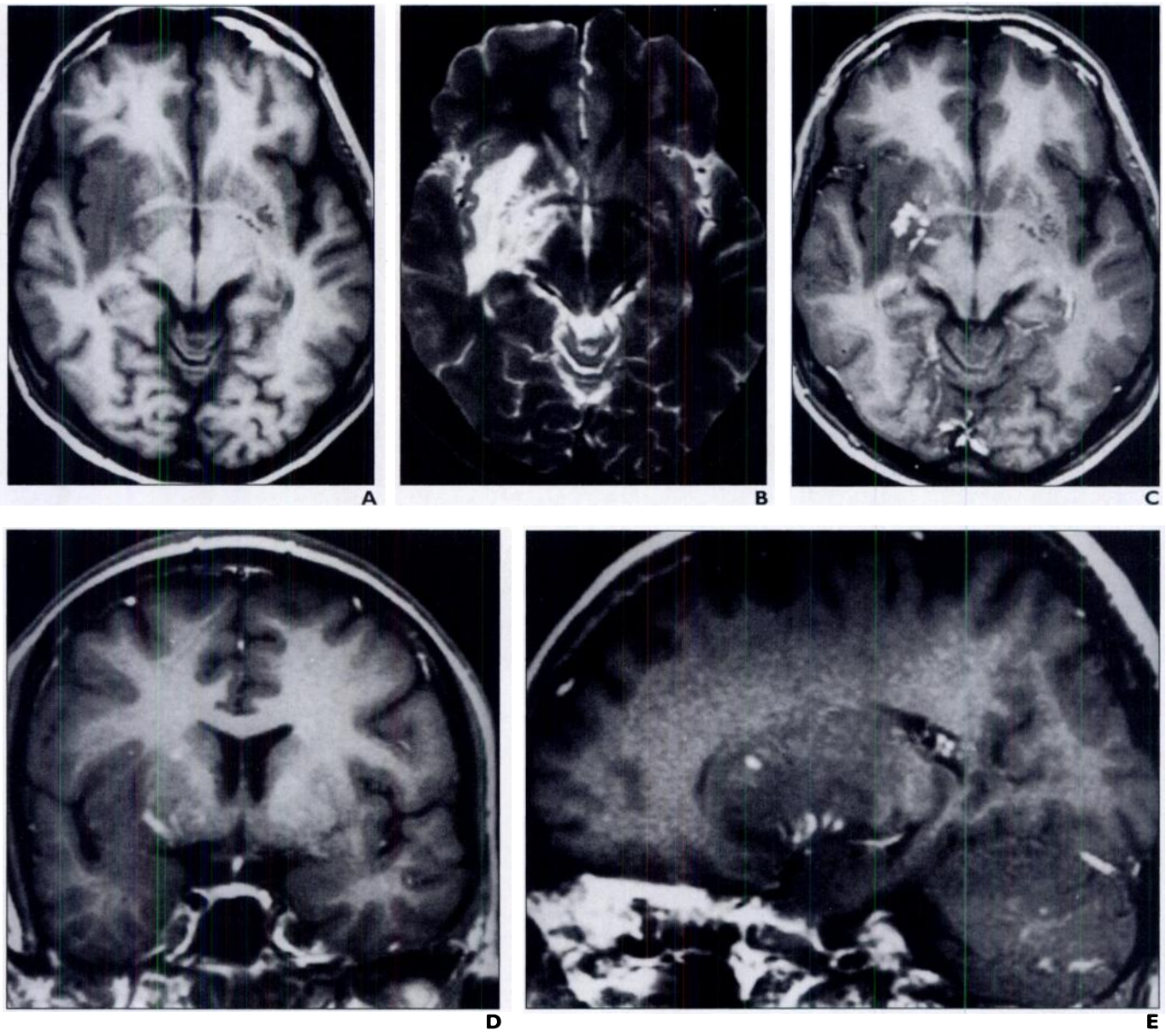

Fig. 3.—29-year-old HIV-positive man with headache.
A, Axial T1-weighted MR image of brain.
B, Axial T2-weighted MR image of brain.
C, Contrast-enhanced axial T1-weighted MR image of brain.
D, Contrast-enhanced coronal T1-weighted MR image of brain.
E, Contrast-enhanced sagittal T1-weighted MR image of brain.

Case 4

A 36-year-old woman with no history of disease who presented with diabetic ketoacidosis and a seizure.

Fig. 4.—36-year-old woman with no history of disease who presented with diabetic ketoacidosis and seizure.
A and **B**, Gadolinium-enhanced T1-weighted axial images of brain.
C, Cerebral angiogram.
D and **E**, Gadolinium-enhanced T1-weighted axial images of brain 1 week later.
F, T2-weighted axial image of brain obtained at same time as **D** and **E**.
G and **H**, Unenhanced (**G**) and contrast-enhanced (**H**) CT images of chest.

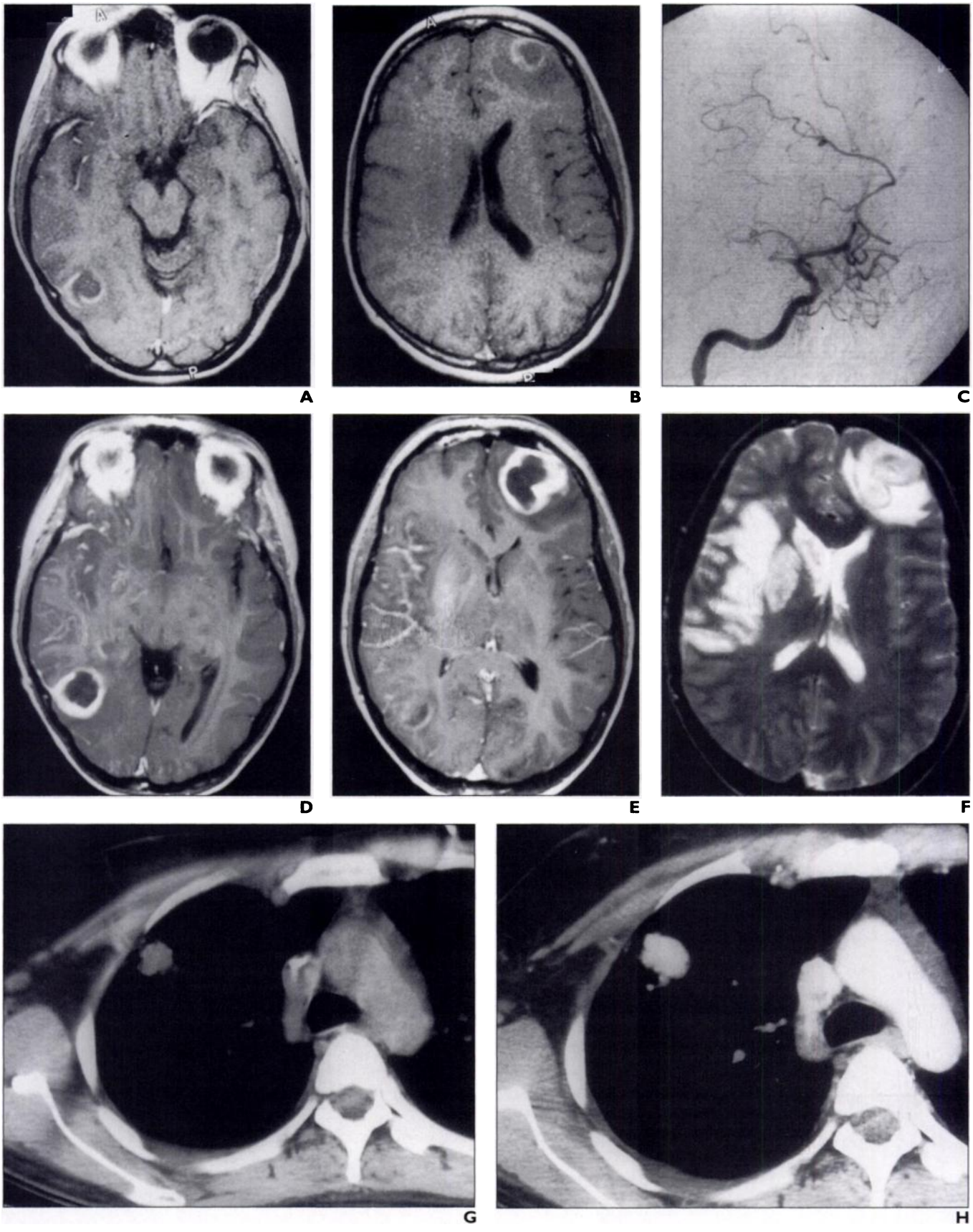

Case 1: Dysembryoplastic Neuroepithelial Tumor

Dysembryoplastic neuroepithelial tumor (DNT) is a benign neuroglial tumor that is predominately cortical but generally extends to involve the adjacent subcortical white matter. DNT is a recently recognized entity, having been introduced into the literature in 1988 by Daumas-Duport et al. [1]. The presenting symptom is almost invariably complex partial seizures, often intractable [2–4]. The most common location is the temporal lobe, although frontal lobe DNTs and, rarely, parietooccipital DNTs have been described [5]. The tumors are always supratentorial.

DNTs are composed of a complex, multinodular architecture and are often described as being associated with focal cortical dysplasia [1, 6]. The male:female ratio varies. Presentation is almost always in childhood or early adolescence, but the age range is broadening as the entity becomes more widely recognized.

On MR images, the tumor has a multilobulated appearance, as in the case presented here (Fig. 1) with signal that is of low intensity on T1-weighted images and of high intensity on T2-weighted images [7]. The lesions are well demarcated 50–80% of the time. Generally, associated edema is not significant and mass effect is only mild, although remodeling of the adjacent calvaria has been described in up to 60% of cases [5, 7]. Gadolinium enhancement occurs in approximately one third of all DNTs but is not a prominent feature (Fig. 1).

The differential diagnosis includes gangliogliomas or other low-grade gliomas, but these neoplasms do not have the propensity for cortical involvement seen with DNTs. On CT images, DNTs appear as low-attenuation, lobu-

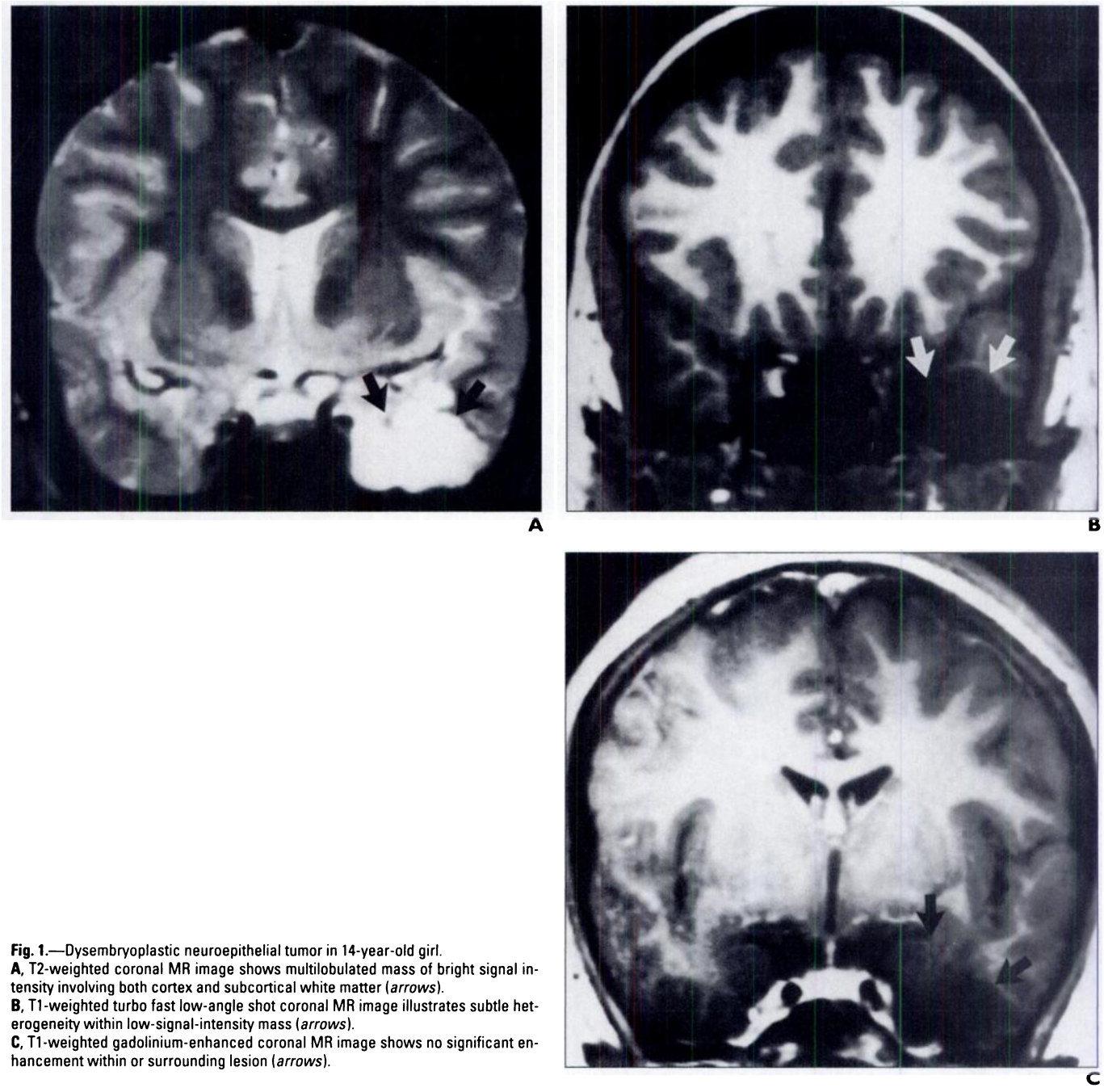

Fig. 1.—Dysembryoplastic neuroepithelial tumor in 14-year-old girl.
A, T2-weighted coronal MR image shows multilobulated mass of bright signal intensity involving both cortex and subcortical white matter (*arrows*).
B, T1-weighted turbo fast low-angle shot coronal MR image illustrates subtle heterogeneity within low-signal-intensity mass (*arrows*).
C, T1-weighted gadolinium-enhanced coronal MR image shows no significant enhancement within or surrounding lesion (*arrows*).

lated masses exhibiting infrequent contrast enhancement. Calcification is seen in fewer than 25% of cases [6].

Recognition of DNT is important because surgical resection is almost always curative. Long-term survival has been established even in cases of incomplete resection [1, 7]. Tumor recurrence has not been reported.

References

1. Daumas-Duport C, Scheithauer BW, Chadkiewicz JP, et al. Dysembryoplastic neuroepithelial tumor: a surgically curable tumor of young patients with intractable partial seizures. *Neurosurgery* **1988**;23: 545–556
2. Vali AM, Clarke MA, Kelsey A. Dysembryoplastic neuroepithelial tumour as a potentially treatable cause of intractable epilepsy in children. *Clin Radiol* **1993**;47:255–258
3. Kirkpatrick PJ, Honavar M, Janota I, Polkey CE. Control of temporal lobe epilepsy following en bloc resection of low-grade tumors. *J Neurosurg* **1993**; 78:19–25
4. Morris HH, Estes ML, Gilmore R, et al. Chronic intractable epilepsy as the only symptom of primary brain tumor. *Epilepsia* **1993**;34:1036–1043
5. Taratuto AL, Pomata H, Sevlever G, et al. Dysembryoplastic neuroepithelial tumor: morphological, immunocytochemical, and deoxyribonucleic acid analysis in a pediatric series. *Neurosurgery* **1995**;36: 474–481
6. Ostertun B, Wolf HK, Manuel G, et al. Dysembryoplastic neuroepithelial tumors: MR and CT evaluation. *AJNR* **1996**;17:419–430
7. Kuroiwa T, Bergey GK, Rothman MI, et al. Radiologic appearance of the dysembryoplastic neuroepithelial tumor. *Radiology* **1995**;197: 233–238

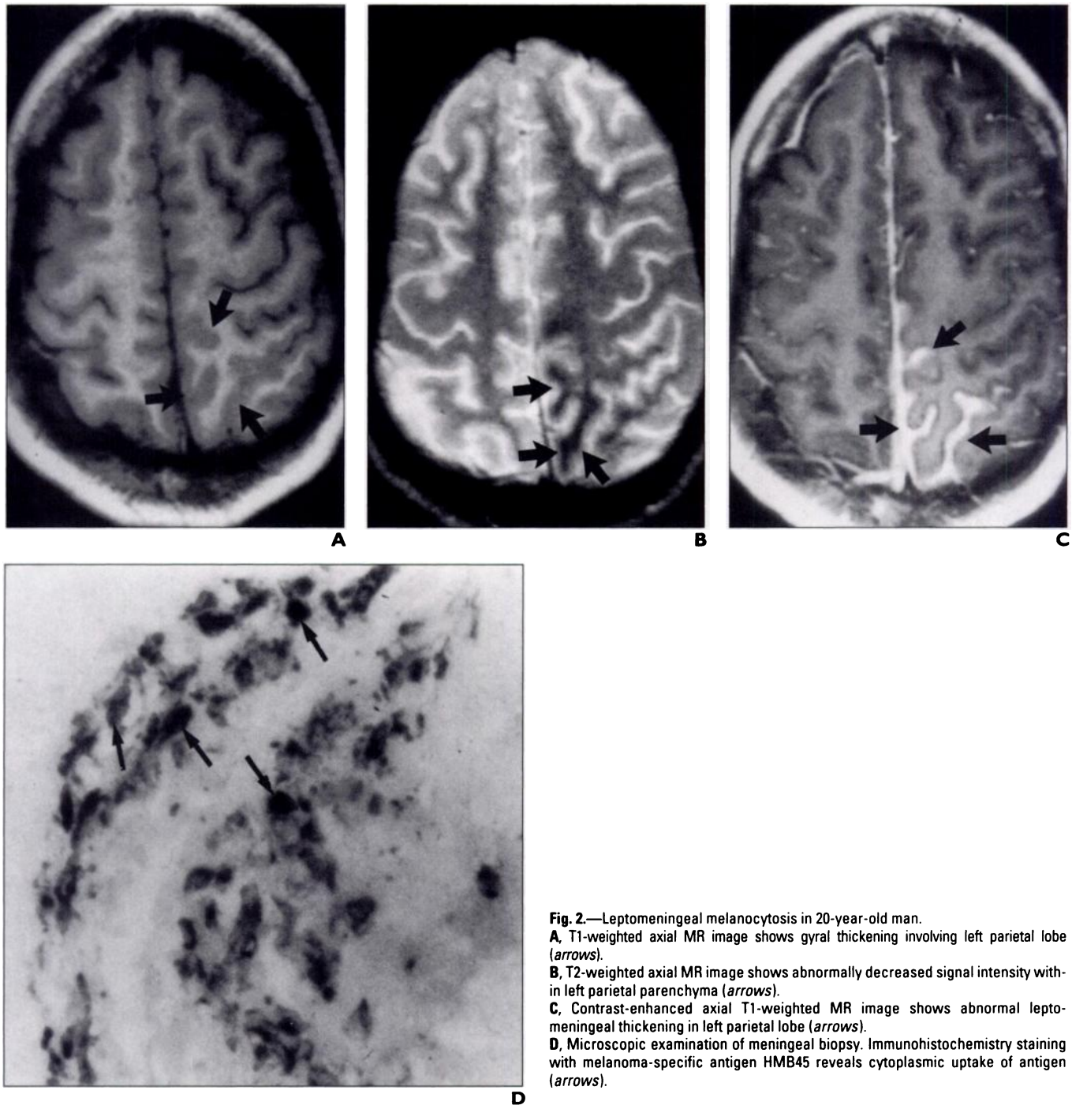

Fig. 2.—Leptomeningeal melanocytosis in 20-year-old man.
A, T1-weighted axial MR image shows gyral thickening involving left parietal lobe (*arrows*).
B, T2-weighted axial MR image shows abnormally decreased signal intensity within left parietal parenchyma (*arrows*).
C, Contrast-enhanced axial T1-weighted MR image shows abnormal leptomeningeal thickening in left parietal lobe (*arrows*).
D, Microscopic examination of meningeal biopsy. Immunohistochemistry staining with melanoma-specific antigen HMB45 reveals cytoplasmic uptake of antigen (*arrows*).

Case 2: Leptomeningeal Melanocytosis

Neurocutaneous melanocytosis refers to a dysplasia of melanin-producing neural crest–derived cells. This disease covers a spectrum from proliferation of benign nevus cells to frank leptomeningeal melanoma. Melanoblasts arise in the neural crest and migrate to the skin, ocular structures, inner ear, and leptomeninges [1]. Leptomeningeal melanocytosis probably arises from a proliferation of these cells. In approximately 40–50% of patients with leptomeningeal melanocytosis, primary meningeal melanomas develop [2].

Neurocutaneous melanocytosis is usually sporadic, although autosomal-dominant cases have been reported [3]. Leptomeningeal melanocytosis is described primarily in children, whereas primary leptomeningeal melanoma is seen in older age groups. In 220 cases reviewed by Allcut et al. [4], the peak age of patients presenting with leptomeningeal melanoma was in the fourth decade.

The proliferating cells in leptomeningeal melanocytosis may disrupt CSF flow dynamics and lead to hydrocephalus, particularly in children. Consequently, the symptoms at presentation are often the same as for increased intracranial pressure, including headache, vomiting, visual changes, and lethargy. Encasement of cranial nerves may produce multiple cranial neuropathies. As in metastatic melanoma, intratumoral hemorrhage is common.

As with most leptomeningeal processes, MR imaging is the diagnostic imaging technique of choice [5]. MR imaging may have normal findings but often shows meningeal thickening, studding, or meningeal-based mass lesions. The meningeal disease may have a characteristic increased signal intensity on unenhanced T1-weighted images or decreased signal intensity on T2-weighted sequences, reflecting the paramagnetic properties of mature melanin. In the case presented (Fig. 2), abnormal decreased signal intensity on T2-weighted images was seen in the parietal lobe parenchyma. This finding was most likely due to the paramagnetic effects of melanin in the adjacent pial infiltration. The lesions enhance after gadolinium administration [6].

Although CSF samples may reveal elevated levels of 5-S-cysteinyldopa, definitive diagnosis usually requires meningeal biopsy [7]. Histologic material reveals a proliferation of pigmented cells [4]. Immunohistochemistry may be useful. The melanotic cells reveal cytoplasmic reactivity to melanoma-specific antigen HMB45, neuron-specific enolase, and S-100.4.

The natural history of neurocutaneous melanocytosis is not well understood, in part because of the relative rarity of the disorder. In addition, as already mentioned, the disorder covers a spectrum of melanocytic proliferative disease. Whereas diffuse leptomeningeal melanoma is probably rapidly fatal, whether there are cases of leptomeningeal melanocytosis that are more indolent is unclear. In the series of eight children with leptomeningeal melanoma of Allcut et al. [4], survival times ranged from 1 to 54 months. Kiel et al. [8] reported a mean survival of 5 months.

References

1. Balmaceda CM, Fetell MR, Powers J, et al. Nevus of ota and leptomeningeal melanocytic lesions. *Neurology* **1993**;43: 381–386
2. Fox H. Neurocutaneous melanosis. In: Vinken PJ, Brwyn EW, eds. *Handbook of clinical neurology*. New York: Elsevier, **1972**:414–428
3. Rubenstein LJ. Neurocutaneous melanosis and primary meningeal melanomas. In: Rubenstein LJ, ed. *Tumors of the central nervous system*. Washington, DC: AFIP, **1972**:309–311
4. Allcut D, Michowiz S, Weitzman S, et al. Primary leptomeningeal melanoma: an unusually aggressive tumor in childhood. *Neurosurgery* **1993**;44: 175–176
5. Fukui MB, Moltze CC, Kanal E, et al. MR imaging of the meninges. II. Neoplastic disease. *Radiology* **1996**:201:605–612
6. Poe LB, Roitberg D, Galyou DD, et al. Neurocutaneous melanosis presenting as an intradural mass of the cervical canal: magnetic resonance features and the presence of melanin as a clue to diagnosis—case report. *Neurosurgery* **1994**; 35:741–743
7. Kamei S, Morishima T, Mizutani T, et al. Measurement and cytologic demonstration of 5-S-cysteinyldopa for the clinical diagnosis of primary leptomeningeal melanoma. *Neurology* **1994**;44: 175–176
8. Kiel FW, Starr LB, Hansen JL, et al. Primary melanoma of the spinal cord. *J Neurosurg* **1961**;18: 616–620

Case 3: CNS Cryptococcal Infection

Cryptococcus neoformans is the most common fungal infection involving the CNS. It is particularly important in patients with AIDS, because in 5% of such patients cryptococcal infection develops. *C. neoformans* is the third most frequent CNS pathogen in patients with AIDS, ranking after HIV and *Toxoplasma gondii* [1].

Dilated perivascular spaces in the basal ganglia are the most common imaging findings noted with CNS cryptococcosis. These findings are better seen on MR images than on CT scans. The dilated perivascular spaces often represent several spaces in close proximity to one another. These often contain small cryptococcomas. Typically, the perivascular spaces follow the normal CSF signal-intensity pattern and do not enhance. However, as seen on the right side in this patient (Fig. 3), abnormal enhancement may be seen [2]. Additionally, the perivascular spaces may have a signal isointense to the white matter on T2-weighted images and hypointense to CSF. This finding can be compatible with a cryptococcoma within the perivascular space [3].

Other imaging findings of CNS cryptococcosis may include rare meningeal enhancement consistent with cryptococcal meningitis and, rarely, intraparenchymal enhancing lesions compatible with larger cryptococcomas. Again, however, contrast enhancement of cryptococcomas or cryptococcal meningitis is rare, most likely because of the underlying immunosuppression of AIDS patients or the nonimmunogenic nature of the polysaccharide capsule of the cryptococcal organism [4].

In summary, this case shows the finding of dilated perivascular spaces in the basal ganglia bilaterally, a common imaging finding with CNS cryptococcosis. The abnormal enhancement of the right perivascular spaces is a relatively rare finding in CNS cryptococcosis and represents enhancement of small cryptococcomas within the perivascular spaces. As noted for the T2-weighted images, the right-sided perivascular spaces do not match the signal intensity of CSF, as do those on the left.

References

1. Mathews VP, Piero AL, Glass JD, et al. AIDS-related CNS cryptococcosis: radiologic-pathologic correlation. *AJNR* **1992**:13:1477–1486
2. Arnder L, Castillo M, Heinz ER, et al. Unusual pattern of enhancement in cryptococcal meningitis: in vivo findings with postmortem correlation. *J Comput Assist Tomogr* **1996**;20:1023–1026
3. Schmidt S, Reiter-Owonda I, Hotz M, et al. An unusual case of central nervous system cryptococcosis. *Clin Neurol Neurosurg* **1995**;97:23–27
4. Takasu A, Taneda M, Otuki H, et al. GD-DTPA-enhanced MR imaging of cryptococcal meningoencephalitis. *Neuroradiology* **1991**;33:443–446

Case 4: Multiple Cerebral Abscesses Associated with Isolated Pulmonary Arteriovenous Malformation

The patient was a previously healthy 36-year-old woman who presented to an outside

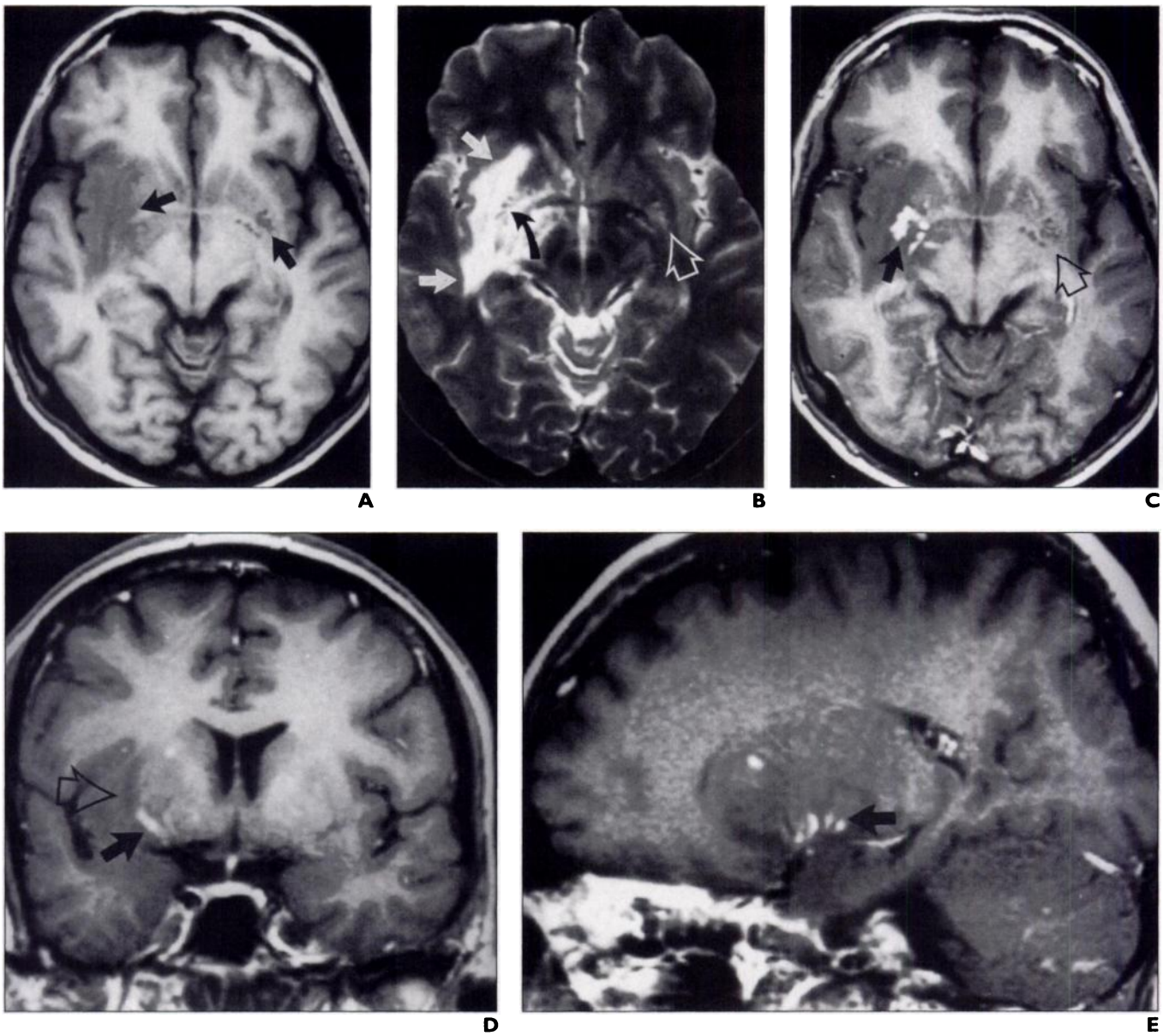

Fig. 3.—CNS cryptococcal infection in 29-year-old man.
A, Axial T1-weighted MR image of brain shows dilated perivascular spaces in basal ganglia bilaterally (*arrows*).
B, Axial T2-weighted MR image of brain shows edema about right lentiform nucleus, right internal and external capsules, and right subinsular cortex (*solid white arrows*). Dilated perivascular spaces on right are isointense to white matter and hypointense to CSF (*curved arrow*). Dilated perivascular spaces on left are isointense to CSF and hyperintense to white matter (*open arrow*).
C, Axial T1-weighted image of brain after gadolinium contrast administration shows abnormal enhancement of dilated perivascular spaces on right, compatible with enhancement of small cryptococcomas within perivascular space (*solid arrow*). No abnormal enhancement on left is seen (*open arrow*).
D and **E**, Coronal (**D**) and sagittal (**E**) T1-weighted images of brain after gadolinium contrast enhancement show enhancing cryptococcomas (*solid arrows*) at base of dilated perivascular spaces on right (*open arrow*, **D**).

hospital with diabetic ketoacidosis and seizures. A head CT scan (not shown) obtained at admission showed the possibility of rim-enhancing lesions in the left frontal and right occipital lobes. A chest radiograph (not shown) obtained at admission showed a possible mass in the right upper lobe.

The patient deteriorated rapidly and was transferred to our hospital, where an MR image was obtained, confirming the ring-enhancing lesions in the right occipital lobe and left frontal lobe. Because of the coexistence of the lung mass, metastasis was suspected. Shortly after admission, the patient suffered an extensive stroke, and emergent cerebral angiography was performed, which showed nearly complete occlusion of the right branches of the middle cerebral and anterior cerebral arteries. Because of the proximal irregularity of the middle cerebral and anterior cerebral arteries, vasculitis was suspected. Repeated MR imaging showed rapid progression of the rim-enhancing lesions, with enhancement greater laterally than medially (Figs. 4D and 4E). Interval development of intense gyral enhancement was seen in the right parietal lobe and right basal ganglia. A brain biopsy was

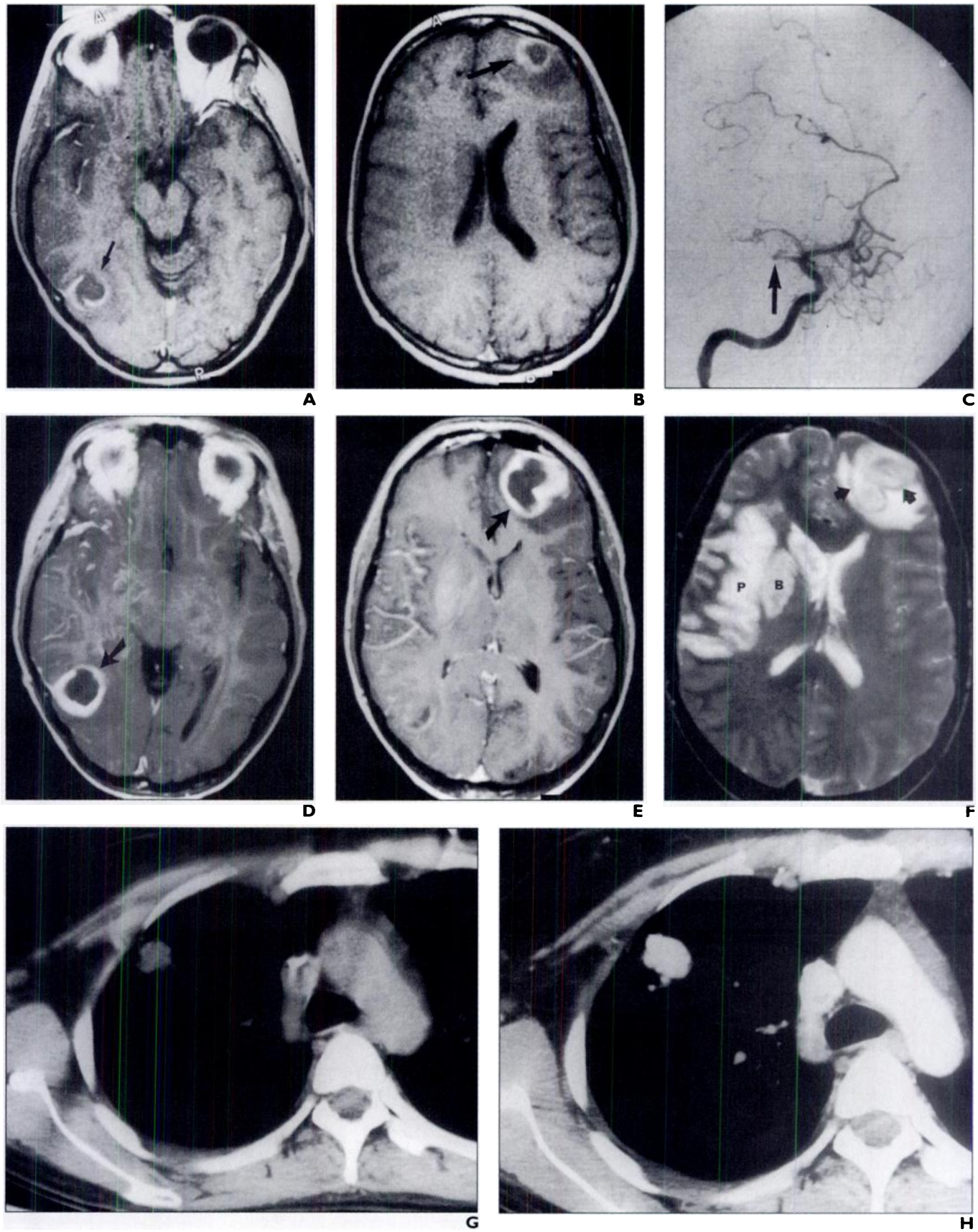

Fig. 4.—Multiple cerebral abscesses associated with isolated pulmonary arteriovenous malformation in 36-year-old woman.
A and **B**, Gadolinium-enhanced T1-weighted axial images of brain show multiple ring-enhancing lesions in right occipital lobe and left frontal lobe (*arrows*).
C, Cerebral angiogram shows cutoff of middle cerebral and anterior cerebral arteries, with irregular narrowing of their origins (*arrow*).
D and **E**, Gadolinium-enhanced images of brain 1 week later show rapid progression of ring-enhancing lesions in brain. Medial rim of enhancement is thinner than its lateral aspect (*arrows*). Extensive cortical enhancement of right parietal lobe and right basal ganglia is seen.
F, Axial T2-weighted images confirm extensive right basal ganglia (B) and right parietal lobe (P) infarction. Note thin low-signal-intensity rim (*arrows*) around frontal lesion.
G and **H**, Unenhanced (**G**) and contrast-enhanced (**H**) chest CT scans show intensely enhancing lobulated mass in right upper lobe of chest.

performed, and pus was aspirated from the left frontal lobe. The patient was begun on antibiotics. A right-to-left shunt was suspected, and a CT scan of the chest revealed an intensely enhancing mass in the right upper lobe with a prominent draining vein, consistent with a pulmonary arteriovenous malformation (AVM) (Figs. 4G and 4H).

Cerebral abscesses represent parenchymal infections contained by a fibrogliotic capsule. Pyogenic bacteria are the most common source, although fungal and parasitic infections do occur. The development of these abscesses implies a breakdown in the blood–brain barrier. Often, cerebral abscesses are associated with traumatic tears of the dura, often from open head trauma. Direct dural extension from paranasal and mastoid sinuses was the most common source before the advent of antibiotics. Currently, hematogenous spread from an extracranial location, often the lung, is the most common cause [1]. The lungs provide an important barrier to the CNS spread of infection; patients with cardiac or systemic shunts are at much greater risk of cerebral infection.

The imaging characteristics of cerebral infection depend on the phase of the infection. In the early cerebritis stage, unenhanced CT scans will show a low-density area, often with a significant mass effect from vasogenic edema [2]. Contrast enhancement varies from thin and irregular to fully rim-enhancing. Because of the differential blood supply of the gray matter–white matter junction, the medial enhancing rim is typically thinner than the thicker cortical rim. MR imaging shows decreased signal intensity from the rim on T1-weighted images and increased signal intensity on T2-weighted images in this early stage. As the abscess organizes, MR imaging shows a characteristic thin, peripheral rim of decreased signal intensity (Fig. 4F) corresponding to the fibrogliotic capsule of the abscess [3]. This dark rim often helps distinguish abscess from enhancing infarcts, metastases, and subacute hematomas.

Patient presentation with an isolated pulmonary AVM is somewhat unusual. Depending on the series, 60–90% of patients with pulmonary AVMs suffer from hereditary hemorrhagic telangiectasia or Osler-Weber-Rendu disease. Depending on the series, approximately 60% of patients exhibit symptoms including dyspnea, cyanosis, and clubbing. Although relatively unusual, CNS events including abscess and stroke are an important cause of morbidity and mortality. In the largest reported series of patients with pulmonary AVMs, 60 of 63 patients showed a pulmonary arteriovenous connection, with three of 63 exhibiting a systemic arterial supply. Although most pulmonary AVMs are single, multiple AVMs are reported in one third of patients. Most patients with pulmonary AVMs present with a round or lobulated subpleural mass, with 70% of the masses located in the lower lobes [4]. Higgins and Wexler [5] further characterized pulmonary AVMs into simple and complex types. Simple pulmonary AVMs consisted of a single artery and draining vein and were seen in 79% of patients in their series, with the remainder showing multiple arterial feeding vessels. Traditionally, symptomatic pulmonary AVMs were treated surgically by lobectomy or pneumonectomy. In 1978, Taylor et al. [6] described the use of embolization coils to successfully treat a simple isolated pulmonary AVM [6]. Castaneda-Zuniga et al. [7] and later White et al. [8] described a successful treatment of multiple pulmonary AVMs with balloon occlusion devices. Current advances in helical CT have improved the diagnosis and presurgical evaluation of pulmonary AVMs and have enabled noninvasive evaluation of these difficult pulmonary lesions [9].

References

1. Zimmerman RD, Weingarten K. Neuroimaging of cerebral abscesses. *Neuroimaging Clin N Am* **1991**; 1:1–16
2. Enzmann DR. Central nervous system infections. In: Harwood-Nash D, ed. *Diagnostic categorical course in neuroradiology*. Chicago: Radiological Society of North America, **1987**; 21–30
3. Enzmann DR, Britt RH, Placone R. Staging of human brain abscess by computed tomography. *Radiology* **1983**;146:703–708
4. Dines DE, Arms RA, Burnatz PE, et al. Pulmonary arterial venous fistulas. *Mayo Clin Proc* **1974**; 49:460–465
5. Higgins C, Wexler L. Clinical and angiographic features of pulmonary arteriovenous fistulas in children. *Radiology* **1976**;119:171–175
6. Taylor BG, Cockerill EM, Manfredi F, et al. Therapeutic embolization of the pulmonary artery in pulmonary arteriovenous fistulas. *Am J Med* **1978**;54:360–365
7. Castaneda-Zuniga W, Epstein M, Zollikoter C, et al. Embolization of multiple pulmonary artery fistulas. *Radiology* **1980**;134:309–310
8. White RI, Mitchell SE, Barth KH, et al. Angioarchitecture of pulmonary malformations: an important consideration before embolotherapy. *AJR* **1983**;140:681–686
9. Remy J, Remy-Jardin M, Giraud F, et al. Angioarchitecture of pulmonary arteriovenous malformations: clinical utility of 3-dimensional helical CT. *Radiology* **1994**;191:657–664